Paper 121

Proceedings of the Eighth International Conference
on Engineering Computational Technology,
B.H.V. Topping, (Editor),
Civil-Comp Press, Stirlingshire, Scotland

A Boundary Element Method for the Computation of Unsteady Sheet Cavitation Effects in Marine Propeller Flows

M. Bauer and M. Abdel-Maksoud
Institute for Fluid Dynamics and Ship Theory
Hamburg University of Technology, Germany

Abstract

This paper focuses on the modelling and simulation of unsteady sheet cavitation in marine propeller flows. In the first part of the paper, the mathematical model based on potential flow theory is introduced and the numerical scheme is derived. The novelty of the presented calculation method refers to the unsteady partial sheet cavitation model which has been implemented into the in-house panel code *pan*MARE [1]. Cavitation is a physical effect where the pressure in the flow falls below the vapour pressure such that a vapour region develops on propeller blades. Cavitation has a significant influence on propeller's performance and can cause material damages, noise and vibrations on the ship hull. In the second part of the paper the capabilities of the developed sheet cavitation model are demonstrated by numerical studies on a three-dimensional foil as well as on a marine propeller flow.

Keywords: sheet cavitation, unsteady cavitation model, boundary element method, panel method, potential theory, propeller flow.

1 Introduction

This paper is dedicated to the numerical investigation of unsteady hydrodynamic characteristics of a marine propeller under cavitating conditions. For the numerical investigation of propeller characteristics a boundary element method based on potential flow theory is used in this work. The governing equations for the propeller flow are derived from the assumption that within a flow domain Ω the flow around a solid body is irrotational, inviscid and incompressible. Since the flow is incompressible the total velocity potential must fullfill the three-dimensional time-dependent Laplace's equation which describes the conservation of mass [2]:

$$\Delta\Phi^*(\vec{x},t) = \nabla^2\Phi^*(\vec{x},t) = 0,\ \forall\,\vec{x} \in \Omega \in \mathbf{R}^3,\ t \in \mathbf{R}^+ \tag{1}$$

where Φ^* is the total velocity potential which is composed of the disturbed potential Φ and the undisturbed free stream potential Φ_∞. The velocity distribution in the flow is obtained by differentiating the total potential:

$$\nabla\Phi^*(\vec{x},t) = \vec{V}(\vec{x},t) = \vec{v}_{ind}(\vec{x},t) + \vec{V}_\infty(\vec{x},t),\ \forall\,\vec{x}\in\Omega,\ t\in\mathbf{R}^+$$

where $\vec{v}_{ind}$ describes the velocity induced by propeller and $\vec{V}_\infty$ is the reference velocity which is the sum of the propeller rotational speed and the inflow velocity to the propeller behind the ship. After having calculated the velocity field, the pressure on the body surface can be calculated by the unsteady Bernoulli equation which describes the conservation of momentum for an incompressible and inviscid fluid [2]:

$$p(\vec{x},t) = p_\infty + \frac{1}{2}\rho(|\vec{V}_\infty(\vec{x},t)|^2 - |\vec{V}(\vec{x},t)|^2) - \rho\frac{\partial\Phi(\vec{x},t)}{\partial t} + \rho g(z_\infty - z),\ t\in\mathbf{R}^+, \quad (2)$$

$\forall\,\vec{x}\in S_B$, where S_B is the body surface, $p_\infty = 101325$ Pa is the constant atmospheric pressure, $\rho = 1000$ kg/m^3 is the water density, $g = 9.81$ m^3/(kg s^2) is the gravity constant and z_∞ is the distance to the free water surface.
In the following sections 2 and 3 the details on the boundary conditions for the modelling of sheet cavitation as well as the numerical scheme used to simulate unsteady cavitating propeller flows are presented. In section 4 several numerical studies are performed and the results obtained by *pan*MARE are compared to the results obtained by other authors.

2 Unsteady sheet cavitation model

2.1 Mathematical formulation

The continuous solution of the Laplace's equation is obtained by Green's third identity as a distribution of sources and dipoles on the body's surface [2]:

$$\Phi(\vec{x}_0,t) = \frac{1}{4\pi}\int_S \Big[\Phi(\vec{x},t)\frac{\partial}{\partial n}\Big(\frac{1}{r(\vec{x}_0,\vec{x})}\Big) - \frac{\partial\Phi(\vec{x},t)}{\partial n}\frac{1}{r(\vec{x}_0,\vec{x})}\Big]dS(\vec{x}) \quad (3)$$

$\forall\,\vec{x}_0\in\Omega$, $S=\partial\Omega$ and $t\in\mathbf{R}^+$. It is common to define the source and dipole strength by the quantities $\sigma(\vec{x},t) := -\partial\Phi(\vec{x},t)/\partial n$ and $\mu(\vec{x},t) := -\Phi(\vec{x},t)$, respectively [2]. There are several approaches to solve equation (3). In the present work a potential based approach is used where the disturbed potential Φ is calculated directly and only evaluation points inside the body are considered. Since there is no disturbed potential inside a solid body, the value of the inner potential can be chosen arbitrary. By setting $\Phi = 0$ inside the body, equation (3) results in:

$$\int_S \Big[\mu(\vec{x},t)\frac{\partial}{\partial n}\Big(\frac{1}{r(\vec{x}_0,\vec{x})}\Big) - \frac{\sigma(\vec{x},t)}{r(\vec{x}_0,\vec{x})}\Big]dS(\vec{x}) = 0,\ \forall\,x_0\in\Omega_{inner} \quad (4)$$

where Ω_{inner} is a subset of Ω which contains only points inside the body. To obtain a unique solution of the above equation, boundary conditions are required on the boundaries of the flow domain Ω. The boundaries which are considered in this paper are the solid propeller surface S_B, the propeller wake surface S_W, the sheet cavitation surface S_C and the cavitating part of the body surface S_{B_C}, respectively (cf. Figure 1). The boundary conditions of the sheet cavitation model will be applied not on the exact cavity sheet S_C but on the corresponding cavitating parts of the body surface, denoted by S_{B_C}. This approach is called the partially non-linear approach [3].

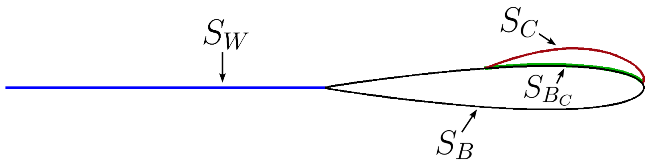

Figure 1: Boundaries of the flow domain Ω

2.1.1 Boundary conditions on the wetted part of the body and wake surface

There are two boundary conditions on the non-cavitating parts of the body and wake surfaces:

(1) On the body surface S_B the Neumann boundary condition is applied which postulates that there is no inflow through a solid surface:

$$\nabla\Phi^*(\vec{x},t)\cdot\vec{n}=0,\ \forall\,\vec{x}\in S_B,\ t\in\mathbf{R}^+ \tag{5}$$

where the vector $\vec{n}$ represents the normal vector on the point $\vec{x}$. From the Neumann boundary condition a relation for the source strength σ on the wetted part of a lifting body can be derived:

$$\sigma(\vec{x},t)=\frac{\partial\Phi_\infty(\vec{x},t)}{\partial n}=\vec{V}_\infty\cdot\vec{n},\ \forall\,\vec{x}\in S_B, t\in\mathbf{R}^+. \tag{6}$$

Hence, the Neumann boundary condition determines the value of the source strengths on the wetted surface of a lifting body, whereas the dipole strengths are still unknown quantities and have to be calculated by solving the integral equation (4).

(2) On the wake surface S_W the physical Kutta condition is applied to model the vorticity shed into the trailing wake of a propeller blade. This condition guarantees that there is no circulation at the trailing edge of a solid body:

$$\Delta p(\vec{x},t)=0,\ \forall\,\vec{x}\in S_W\, t\in\mathbf{R}^+ \tag{7}$$

where $\Delta p=p^+-p^-$ is the pressure difference between the pressure value on the upper and lower side of the trailing wake. By means of the Kutta condition the dipole strengths on the wake surface can be determined. The dipole strengths on the trailing wake are defined by $\Delta\Phi(\vec{x},t) = \Phi(\vec{x}^{+},t) - \Phi(\vec{x}^{-},t) = -\mu_{wake}(\vec{x},t)$ where $\Phi(\vec{x}^{+},t)$ and $\Phi(\vec{x}^{-},t)$ are the potentials on the upper and lower side of the wake, respectively.

2.1.2 Boundary conditions on the cavitating part of the body surface

The boundary conditions for sheet cavitation will be formulated in a surface-fitted local non-orthogonal coordinate system with the base unit vectors $\vec{t_1}$, $\vec{t_2}$, $\vec{t_3}$ and local coordinates described by $\vec{s} = (s_1, s_2, s_3)$. The reason for using a surface-fitted local coordinate system is the simpler mathematical formulation of the boundary conditions.

For the mathematical description of sheet cavitation two regions are significant, the region where cavitation starts and the region where cavitation ends. The starting point of cavitation is called the detachment point and will be denoted by $\vec{s}_{d.p.}$, the cavity closure point is called the reattachment point and will be denoted by $\vec{s}_{r.p.}$. The location of the detachment as well as the reattachment points are not known a priori and have to be determined by an algorithm or have to be estimated by an empirical formula. In the present work the detachment point is estimated by the Villat-Brillouin criterion [4]. The reattachment point is calculated by an iterative procedure which will be presented in section 3.

Now, on the cavitating body surface S_{B_C} two boundary conditions are formulated:

(1) The kinematic boundary condition which postulates that there is no inflow through the cavity sheet:

$$\frac{D}{Dt}F(\eta(s_1, s_2, t), s_3) = 0, \; \forall\, \vec{s} = (s_1, s_2, s_3) \in S_{B_C},\; t \in \mathbf{R}^+ \tag{8}$$

where η is the cavity thickness and $F(\eta(s_1, s_2, t), s_3) = s_3 - \eta(s_1, s_2, t)$ is a function for the cavity shape. From equation (8) it follows that the continuous kinematic boundary condition is a linear partial differential equation for the unknown cavity thickness η:

$$a\frac{\partial \eta}{\partial s_1}(\vec{s},t) + b\frac{\partial \eta}{\partial s_2}(\vec{s},t) = |\vec{t_1} \times \vec{t_2}|(V_{s_3}(\vec{s},t) - \frac{\partial \eta(\vec{s},t)}{\partial t}),\; \forall\, \vec{s} \in S_{B_C},\; t \in \mathbf{R}^+ \tag{9}$$

where

$$a = (V_{s_1}(\vec{s},t) - (\vec{t_1}\cdot\vec{t_2})V_{s_2}(\vec{s},t)), \quad b = (V_{s_2}(\vec{s},t) - (\vec{t_1}\cdot\vec{t_2})V_{s_1}(\vec{s},t))$$

and $V_{s_i}, i = 1,2,3$ are the velocity components of the total velocity $\vec{V}$ in the local non-orthogonal coordinate system.

(2) The second condition used to describe the physics of sheet cavitation on S_{B_C} is the dynamic boundary condition:

$$p(\vec{s},t) = p_{vapour},\; \forall\, \vec{s} \in S_{B_C},\; t \in \mathbf{R}^+ \tag{10}$$

where p_{vapour} is the vapour pressure of water. By using equation (2), the dynamic boundary condition can be transformed in a Dirichlet like formulation for the velocity potential μ on the cavitating part of the body:

$$\mu(\vec{s},t) = \mu_0(t) - \int_{s_{d.p.,1}}^{s_1} [|\vec{t}_1 \times \vec{t}_2| \sqrt{f(\vec{s},t)} + \vec{t}_1 \cdot \vec{t}_2 V_{s_2}(\vec{s},t) - V_{\infty,s_1}(\vec{s},t)] ds_1, \quad (11)$$

$\forall \, \vec{s} \in S_{B_C}$, $t \in \mathbf{R}^+$ where $\mu_0(t) = \mu(\vec{s}_{d.p.}, t)$ is the potential at the detachment point of cavitation, the function f is defined by

$$f(\vec{s},t) = |\vec{V}_\infty(\vec{s},t)|^2(1+\sigma_v) + 2g(s_{3,\infty} - s_3) + 2\frac{\partial \mu(\vec{s},t)}{\partial t} - V_{s_2}^2(\vec{s},t) - V_{s_3}^2(\vec{s},t),$$

and σ_v is the dimensionless cavitation number

$$\sigma_v := \frac{p_{ref} - p_{vapour}}{\frac{\varrho}{2}|\vec{V}_\infty|^2}. \quad (12)$$

The normal component of the local velocity V_{s_3} does not have a significant influence on the magnitude of the dipole strength but it can cause numerical instabilities. For that reason it will be neglected in the following numerical considerations [3].

2.2 Numerical formulation

For the numerical simulation the in-house simulation tool *pan*MARE is used. This programme is based on a three-dimensional panel method where the body and wake surfaces are discretised in flat quadrilateral elements and the governing equations of the potential flow problem are applied on a collocation point of each panel element (cf. Figure 2(a), 2(b)). The collocation points are defined in *pan*MARE as the centre points of the surface panels which are slightly displaced inside the body. They will be denoted in the following by $\vec{x}_j$, $\forall \, j = 1, \dots, N$ where N is the number of body panels. The centre points of the body and wake panels will be denoted by $\vec{x}_i$, $\forall \, i = 1, \dots, N, N+1, \dots, N_{wake}$ where N_{wake} is the number of wake panels.
On each body panel element a source and a dipole is distributed with a constant strength over one panel. On the wake panels only dipoles are distributed since no displacement is induced by the wake. Due to the discretisation of the geometry, equation (4) results in a linear equation for each collocation point x_j, $j = 1, \dots, N$:

$$\sum_{i=1}^{N+N_{wake}} \mu_i^n A_{i,j} - \sum_{i=1}^{N} \sigma_i^n B_{i,j} = 0, \quad (13)$$

where $\mu_i^n := \mu(\vec{x}_i, t_n)$, $\sigma_i^n := \sigma(\vec{x}_i, t_n)$ are the discrete dipole and source strength for the discrete time step t_n and

$$A_{i,j} := A(\vec{x}_i, \vec{x}_j) = \int_{Panel_i} \frac{\partial}{\partial n} \frac{1}{r(\vec{x}_j, \vec{x}_i)} dS(\vec{x}_i), \quad \forall \, i = 1, \dots, N, \dots, N + N_{wake},$$

$$B_{i,j} := B(\vec{x}_i, \vec{x}_j) = \int_{Panel_i} \frac{1}{r(\vec{x}_j, \vec{x}_i)} dS(\vec{x}_i), \quad \forall \, i = 1, \dots, N,$$

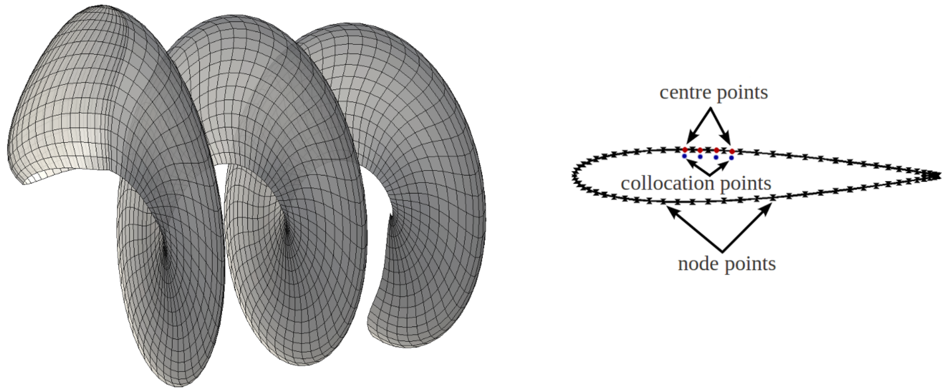

(a) Discretised propeller blade and wake

(b) Centre, collocation and node points on a blade profile

Figure 2: Discretisation of the geometry

$\forall\, j = 1, \ldots, N$ are the influence functions which describe the dipole or source influence of the panel i on the panel j.

2.2.1 Discrete wetted flow model

Firstly, the wetted flow solution is considered where the bodies are assumed to have no sheet cavitation. Then, the value of the source strength is known from equation (6) and application of (13) on N body collocation points results in a linear system of equations with dimension $N \times (N + N_{wake})$ for $(N + N_{wake})$ unknown dipole strengths at the body and trailing wake surfaces. To handle the problem that the linear system of equations is under-determined the Kutta condition (7) is applied at the trailing edge of the lifting body. There are two possibilities for the numerical use of the Kutta condition. Firstly, the non-linear formulation $\Delta p(\vec{x}_{wake}, t) = 0$ can be used to find the value of the dipole strength $\Delta\Phi_{wake} = -\mu_{wake}$. This approach will result in an iterative procedure since the equation for pressure is a non-linear equation in μ_{wake}. Alternatively, a linear form of the Kutta condition can be formulated:

$$\mu_{wake} = \mu_{upper} - \mu_{lower} \tag{14}$$

where μ_{upper} and μ_{lower} are the dipole strengths of the body panels which are located either at the suction side or at the pressure side of the trailing edge. In this work the linear form of the Kutta condition is applied and the influence functions $A_{i,j}$, $\forall\, i, j =$

$1, \ldots, N$ are substituted in the following way:

$$A^*_{i,j} = A_{i,j} + \sum_{l=1}^{N_{wake}} A_{l,j}, \quad \text{if panel } i \text{ lies on the upper side of the trailing edge,}$$

$$A^*_{i,j} = A_{i,j} - \sum_{l=1}^{N_{wake}} A_{l,j}, \quad \text{if panel } i \text{ lies on the lower side of the trailing edge,}$$

$$A^*_{i,j} = A_{i,j}, \text{ else.}$$

Now, one obtains a linear system of equations of dimension $N \times N$ for the unknown body dipole strengths $\mu_i^n, \forall\, i = 1, \ldots, N$:

$$\begin{pmatrix} A^*_{1,1} & \ldots & A^*_{1,N} \\ \vdots & \vdots & \vdots \\ A^*_{N,1} & \cdots & A^*_{N,N} \end{pmatrix} \begin{pmatrix} \mu_1^n \\ \vdots \\ \mu_N^n \end{pmatrix} = \begin{pmatrix} B_{1,1} & \ldots & B_{1,N} \\ \vdots & \vdots & \vdots \\ B_{N,1} & \cdots & B_{N,N} \end{pmatrix} \begin{pmatrix} \sigma_1^n \\ \vdots \\ \sigma_N^n \end{pmatrix}. \tag{15}$$

Once this linear system of equations is solved, the local velocities can be computed from the relations:

$$V^n_{s_1,i} = -\frac{\partial \mu_i^n}{\partial s_1}, \quad V^n_{s_2,i} = -\frac{\partial \mu_i^n}{\partial s_2}, \quad V^n_{s_3,i} = -\sigma_i^n, \quad \forall\, i = 1, \ldots, N. \tag{16}$$

With the aid of the local velocities the shape of the trailing wake surface can be adjusted. A detailed description of the solution algorithm for the wake alignment can be found in [2].

2.2.2 Discrete cavitating flow model

The novelty of the presented numerical method refers to the unsteady sheet cavitation model implemented in the simulation tool *pan*MARE. The development of a sheet cavitation model is motivated by the effects which can be caused by cavitation of propeller blades. In the presented solution procedure firstly the boundary value problem (15) without sheet cavitation calculation is solved. Then, the pressure distribution is calculated by the Bernoilli equation (2) and a first guess of the cavity length is made by applying the criterion:

$$p(\vec{x}_i, t^n) \leq p_{vapour}, \quad \forall\, i = 1, \ldots N. \tag{17}$$

In the next step, the dipole strengths on the cavitating panels are calculated by discretising the dynamic boundary condition (11):

$$\mu_i^{cav,n} = \mu_0^n + \tilde{\mu}_i^n. \tag{18}$$

The value of μ_0^n is extrapolated from the three dipole values in front of the inception point of sheet cavitation. The value of $\tilde{\mu}_i^n$ is calculated by discretising the integral in equation (11) by means of the trapezoidal rule [3]. The occuring unsteady terms

$\frac{\partial \mu^n}{\partial t}$ and $V_{s_2}^n$ in the dynamic boundary condition can cause numerical problems since their values are not known and have to be estimated by an approximation. For the approximation of the potential gradient an approach from [5] is used. The main idea of that approach is to estimate the potential gradients by differentiating equation (13):

$$\frac{\partial}{\partial t}\Big(\sum_{i=1}^{N+N_{wake}} A_{i,j}\mu_i^n - \sum_{i=1}^{N} B_{i,j}\sigma_i^n\Big) = 0.$$

Since the influence functions depend only on the geometry and does not vary in time, the differential quotient can be put behind the influence coefficients, such that one obtains:

$$\sum_{i=1}^{N+N_{wake}} A_{i,j}\frac{\partial \mu_i^n}{\partial t} - \sum_{i=1}^{N} B_{i,j}\frac{\partial \sigma_i^n}{\partial t} = 0. \tag{19}$$

The change of displacement on the non-cavitating panels should vanish, i.e.

$$\frac{\partial \sigma_i^{noncav,n}}{\partial t} = 0. \tag{20}$$

The value of $\frac{\partial \mu_i^{cav,n}}{\partial t}$ can be determined from equation (11):

$$\frac{\partial \mu_i^{cav,n}}{\partial t} = -\frac{1}{2}|V_{\infty,i}^n|^2(1+\sigma_v) + \frac{1}{2}|V_i^n|^2 - g(z_\infty - z_i^n), \tag{21}$$

whereas the value of $\vec{V}_i^n$ is approximated by its value from the previous time step:

$$\vec{V}_i^n \approx \vec{V}_i^{n-1},\ \forall\, i = 1,\dots,N.$$

After having determined the value of μ on the cavitating panels and by assuming that there are N_{cav} cavitating and $(N - N_{cav})$ non-cavitating panels, the linear system of equations for the cavitating case can be set up:

$$\sum_{i=1}^{N_{noncav}} A_{i,j}^{*}\mu_i^{noncav,n} - \sum_{i=1}^{N_{cav}} B_{i,j}\sigma_i^{cav,n} = -\sum_{i=1}^{N_{cav}} A_{i,j}^{*}\mu_i^{cav,n} + \sum_{i=1}^{N_{noncav}} B_{i,j}\sigma_i^{noncav,n}, \tag{22}$$

$\forall\, j = 1,\dots,N$, where the known parts are put on the right side and the unknown parts on the left side of the system.

3 Solution algorithm

The whole solution algorithm for the calculation of unsteady sheet cavitation on a lifting body can be summarised as follows:

(1) Firstly, the linear system of equations (15) without sheet cavitation calculation is set up and solved numerically.

(2) The velocities and pressures on the body and wake surfaces are calculated by equations (16) and (2) and the initial cavity length is estimated by criterion (17).

(3) The time dependent potential gradients are calculated by solving the linear system of equations (19).

(4) Then, the linear system of equations (22) for cavitating and non-cavitating panels is set up. Hereby, for the computation of the dipole and source strengths the following differentiation is made:

   - On non-cavitating body panels: The source strengths are known in advance from relation (6), the dipole strengths are determined by solving the linear system of equations (22).
   - On cavitating body panels: The dipole strengths are calculated by the discrete dynamic boundary condition (18). The source strengths are determined by solving the linear system of equations (22).
   - On wake panels: The dipole strengths are calculated by applying the Kutta condition (14).

(5) The new velocities and pressures on the cavitating and non-cavitating body and wake panels are calculated by equations (16) and (2).

(6) The cavity thickness on the cavitating parts of the body is computed by solving the partial differential equation (9). For the approximation of the spacial derivatives $\frac{\partial}{\partial s_1}$ and $\frac{\partial}{\partial s_2}$ a central difference scheme and for the approximation of the time derivative a backwards difference scheme of first order is used.

(7) The cavity shape is computed by an iterative procedure. If the computed cavity thickness at the cavity closure is smaller than a given tolerance, the algorithm stops. If it is not the case, a new estimate for the cavity length is made and the steps (3) to (7) are repeated until convergence. The mesh of the body surface is not regridded during the iteration procedure.

At the end, the propeller characteristics can be computed. The force and the moment are calculated by:

$$\vec{F} = -\sum_{i=1}^{N} p(\vec{x}_i, t^n)\vec{n}_i \int_{Panel_i} dS(\vec{x}), \quad \vec{M} = -\sum_{i=1}^{N} p(\vec{x}_i, t^n)(\vec{n}_i \times \vec{x}_i) \int_{Panel_i} dS(\vec{x}).$$

The cavity area and volume are determined by:

$$A_{cav} = \frac{\sum_{i=1}^{N_{cav}} \int_{Panel_i} dS(\vec{x})}{\sum_{i=1}^{N} \int_{Panel_i} dS(\vec{x})}, \; V_{cav} = \frac{\sum_{i=1}^{N_{cav}} \eta(\vec{x}_i, t^n) \int_{Panel_i} dS(\vec{x})}{\sum_{i=1}^{N} \int_{Panel_i} dS(\vec{x})}.$$

4 Simulation results

This section demonstrates the abilities of the implemented sheet cavitation model. For this purpose numerical studies are performed for a three-dimensional unsteady foil flow as well as for an unsteady marine propeller flow.

4.1 Numerical studies on the three-dimensional NACA0010 foil

In the following numerical studies the considered foil section is a NACA0010 with 90 panels along the cross section and 10 panels along the spanwise direction of the foil. In the first study the pressure distribution under subcavitating condition is kept constant and the cavitation number is forced to vary in time. In the second study the cavitation number is kept constant and the angle of attack is varied by forcing a temporal change of the inflow velocity in the normal direction.

4.1.1 Results for the NACA0010 foil in an oscillating cavitation number field

The three-dimensional NACA0010 foil was calculated with the geometrical aspect ratio $\Lambda = \text{span}^2/\text{reference area} = 3$ and angle of attack $\alpha = 5°$. In order to have an oscillating cavitation number and a constant pressure distribution in subcavitating condition, the unsteady potential gradient in the dynamic boundary condition (11) is set to zero and the cavitation number is defined as a function of time:

$$\sigma_v(t) = 0.9259 + 0.2436 \cdot \sin(\omega t). \tag{23}$$

Thus, the cavitation number varies between 1.1695 and 0.6823 (cf. Figure 3). All

Characteristics	Value
α	5 [deg]
V_{inflow}	10 [m/s]
Δt	1/300 [s]
ω	$2\pi \cdot 4$ [1/s]
Blade section	NACA0010
Λ	3

Table 1: Input data for the test case 1

relevant data used in the calculations are summarised in Table 1.
Figures 4 - 6 present the results of the calculations. On Figure 4 the dimensionless pressure distribution for several cavitation numbers is illustrated. The pressure is scaled by the stagnation pressure $-1/2\rho|V_{inflow}|^2$. The graphs on Figure 4 demonstrate that the dimensionless pressure is constant and equal to the cavitation number in the regions where sheet cavitation occurs. These results varify the physical correctness of the implemented model.
On Figure 5 a screenshot of the NACA0010 foil with the calculated cavity sheet and

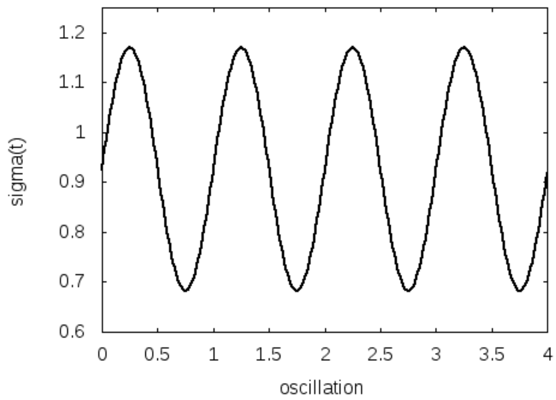

Figure 3: Oscillating cavitation number

thickness determined by *pan*MARE for the cavitation number $\sigma_v = 0.6823$ is presented. Figure 6 illustrates the calculated results for the lift and drag coefficients which are defined by:

$$c_l = \frac{Lift}{1/2\rho|V_{inflow}|^2} \quad c_d = \frac{Drag}{1/2\rho|V_{inflow}|^2}. \tag{24}$$

The results calculated by *pan*MARE confirm qualitatively very well to the results published by [6]. By increasing the cavitation number the lift and drag coefficients decrease until a minimal value is achieved where no sheet cavitation occurs. On the other hand, a deacrease of the cavitation number leads to a rise of the lift and drag coefficient which is due to the increasing sheet cavity length and cavity thickness. As it can be seen in Figure 4 the cavitation area has a strong influence on the pressure distribution. The pressure peak at the leading edge of the suction side of the foil is reduced by cavitation and the cavitation area length is much longer than this pressure peak. In the area of the cavity sheet vapor pressure exists which is lower than the local pressure without cavitation. This pressure reduction increases the lift force on the foil.

4.1.2 Results for the NACA0010 foil in pitch motion

In the second test case the foil was calculated with a varying angle of attack. The varying angle of attack is equivalent to a non-uniform inflow to the foil and the inflow velocity is defined as a function of time:

$$V_{inflow}(t) = V_\infty + V_0 \cdot \sin(\omega t) \tag{25}$$

where $V_\infty = 1$ and V_0 was chosen in the way that the angle of attack varies between $\alpha = +5°$ and $\alpha = -5°$. The calculations were performed for the constant cavitation number $\sigma_v = 0.65$. All relevant data of the simulations are summarised in Table 2. The results of the simulations are demonstrated in Figure 7(a) and compared to the

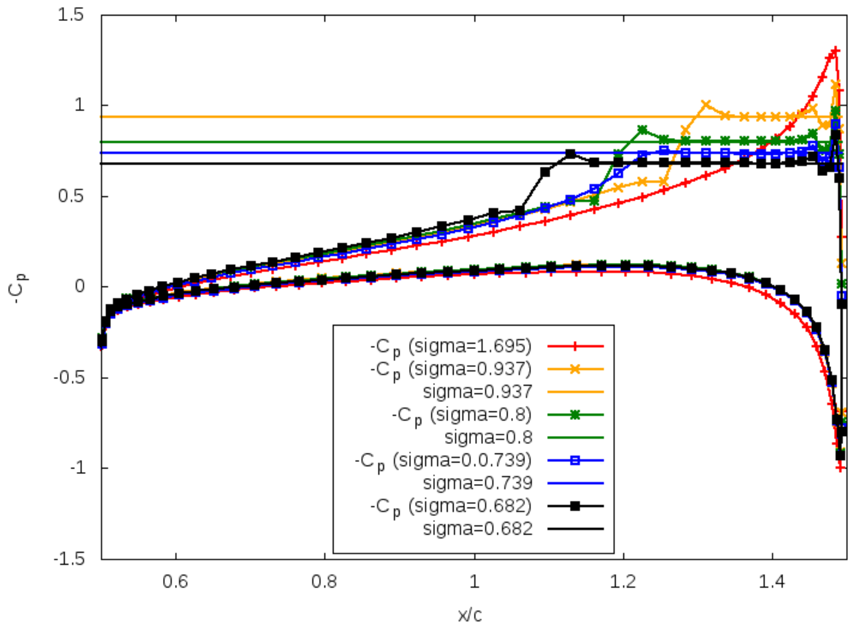

Figure 4: Scaled pressure distribution of the NACA0010 foil in an oscillating cavitation field

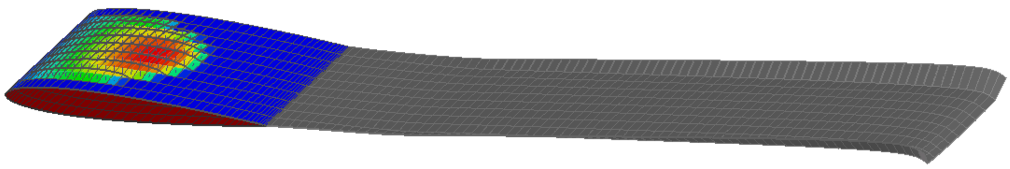

Figure 5: Sheet cavitation thickness on the NACA0010 foil for the cavitation number $\sigma_v = 0.6823$

results obtained by [6] (cf. 7(b)). Figure 7(a) illustrates the lift coefficient for the cavitating and non-cavitating case as a function of the angle of attack. The results show that for the angle of attack between $2°$ and $5°$ the lift coefficient of the foil increases due to the existence of sheet cavitation. These results confirm very well with the results published in [6] (cf. 7(b)). The only difference to the results in 7(b) is that the results of *pan*MARE show no sheet cavitation on the pressure side of the foil. This is because only an algorithm for the computation of the suction side cavitation has been implemented in *pan*MARE, thus the pressure side cavitation cannot be captured by the programme at the moment.

4.2 Numerical studies on the P1356 propeller

In this section the five-bladed marine propeller KCS (MOERI Container ship) is studied under cavitating conditions. All relevant propeller data are listed in Table 3. The

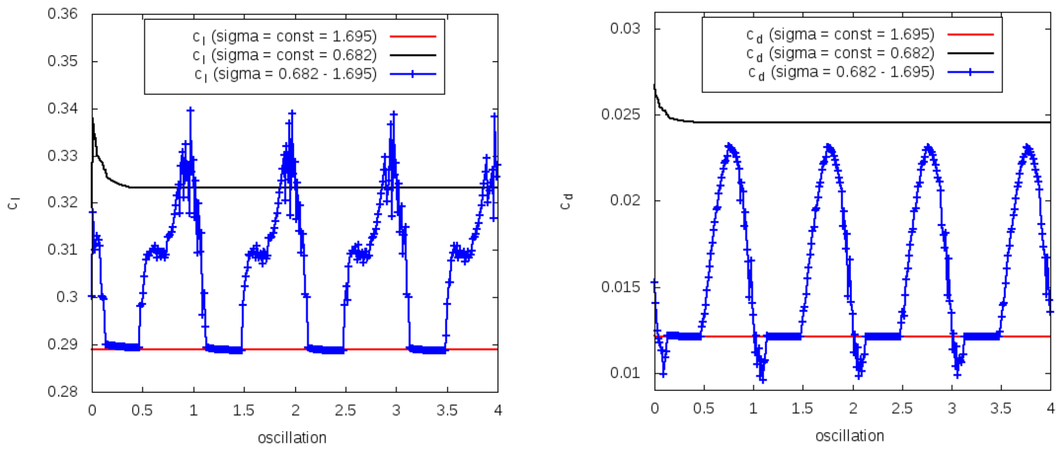

(a) Lift coefficient for an oscillating cavitation number

(b) Drag coefficient for an oscillating cavitation number

Figure 6: Results of the sheet cavitation calculations on the NACA0010 foil for an oscillating cavitation number

Characteristics	**Value**
σ_v	0.65
V_∞	1 [m/s]
V_0	$\pm$0.0875 [m/s]
Δt	1/300 [s]
ω	$1 \cdot \pi$ [1/s]
Blade section	NACA0010
Λ	3

Table 2: Input data for the test case 2

grid of the propeller consists of 20 panels in the spanwise and 70 panels in the crosswise direction. In the following numerical studies the propeller is simulated for two different inflow velocity fields and cavitation numbers.

4.2.1 P1356 propeller with a homogeneous inflow velocity

In the first test case the propeller is simulated with a uniform inflow velocity $V_{inflow} = 4.74$ and the cavitation number $\sigma_v = 6.42$. Figure 8 shows a comparison between the simulation results obtained by *pan*MARE and the experimental results measured by the SVA (Schiffbau-Versuchsanstalt Potsdam GmbH) for the same cavitation number [7]. The cavity shape calculated by *pan*MARE conforms qualitatively very well to the cavity shape measured by the exprement. At the blade tip of the propeller the sheet cavity length calculated by *pan*MARE is a little underestimated. This is due to the fact that no tip vortex cavitation can be calculated in *pan*MARE at the moment.

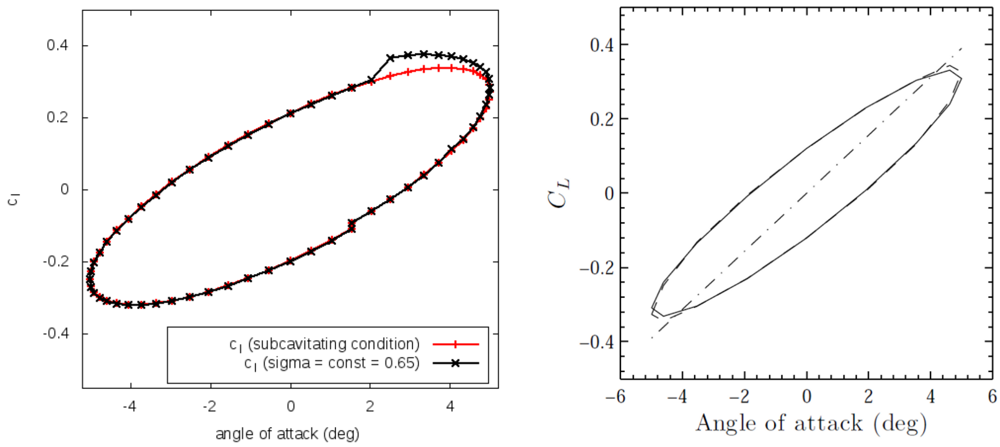

(a) Lift coefficient calculated by *pan*MARE (b) Lift coefficient calculated by [6]

Figure 7: Calculated and measured lift coefficients for the NACA0010 foil in pitch motion

Characteristics	**Value**
Propeller diameter (D_{prop})	0.25 [m]
Hub ratio	0.180
Skew	12.66 [deg]
Mean camber line distribution (a)	0.8
Blade section	NACA66
Pitch ratio	1
Propeller area ratio	0.7
Scale ratio	$\lambda = 31.6$

Table 3: Propeller data

4.2.2 P1356 propeller in a non-uniform wakefield

In the second study the KCS propeller is simulated in a non-uniform wakefield with the constant cavitation number $\sigma_v = 2.651$. The results of the sumulations are shown in Figure 9 for two different angular positions of the key blade and compared to the experimental results measured by the SVA (Schiffbau-Versuchsanstalt Potsdam GmbH) [8]. The results obtained in the simulations are consistent with the experimental results and for both angular positions the cavity shape is calculated correctly.
Additionally, in Figure 10 the relative thrust coefficient of the cavitating KCS propeller is illustrated as a function of the blade angular position. As it can be seen in Figure 10 sheet cavitation has an influence on the thrust coefficient of the propeller. The thrust coefficient of the propeller operating in an unsteady cavitating flow is smaller than that of the non-cavitating propeller.

Advance coefficient	$J = 0.6$
Rotation speed	$n = 25$ [1/s]
Inflow velocity	$V_{inflow} = J \cdot n \cdot D_{prop}$=4.74 [m/s]
ω	$2\pi \cdot n$ [1/s]
Cavitation number	$\sigma_v = 6.42$

Table 4: Input data for the test case 1

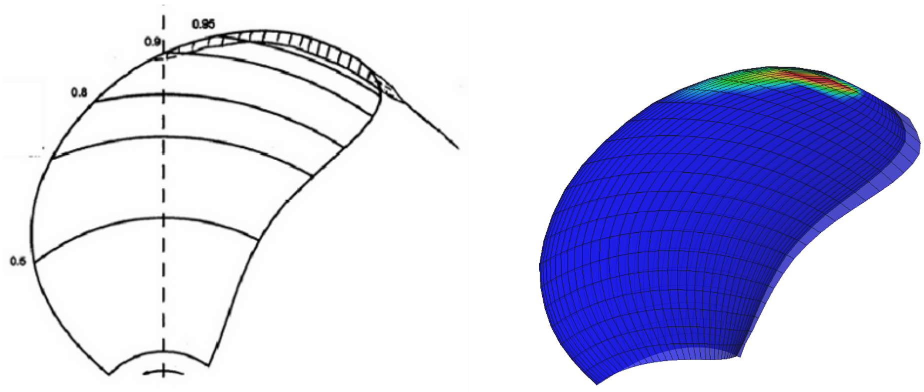

(a) Sheet cavitation measured by SVA [7]

(b) Sheet cavitation calculated by *pan*MARE

Figure 8: Comparison of the measured and calculated results for the sheet cavity on the KCS propeller for $\sigma_v = 6.42$

5 Discussion and outlook

In this paper a calculation scheme for the determination of unsteady sheet cavitation on a hydrofoil and marine propeller flows was devised. The numerical model was implemented in the in-house simulation tool *pan*MARE and applied to a three-dimensional foil flow as well as to a five-bladed marine propeller flow. The numerical results obtained by *pan*MARE show a good agreement with the results obtained by other authors and experiments.

In the next steps, the code should be further validated by two- and three-dimensional examples and the free surface effects should be included in the calculation of the cavity sheet. It was investigated by Bal and Kinnas that the inclusion of a free surface in the numerical calculations may have a significant influence on the cavity shape re-

Advance coefficient	$J = 0.7497$
Rotation speed (n)	$n = 11.72$ [1/s]
Inflow velocity	$V_{ship} = J \cdot n \cdot D_{prop} = 2.196$ [m/s]
ω	$2\pi \cdot n$ [1/s]
Cavitation number	$\sigma_v = 2.651$

Table 5: Input data for the test case 2

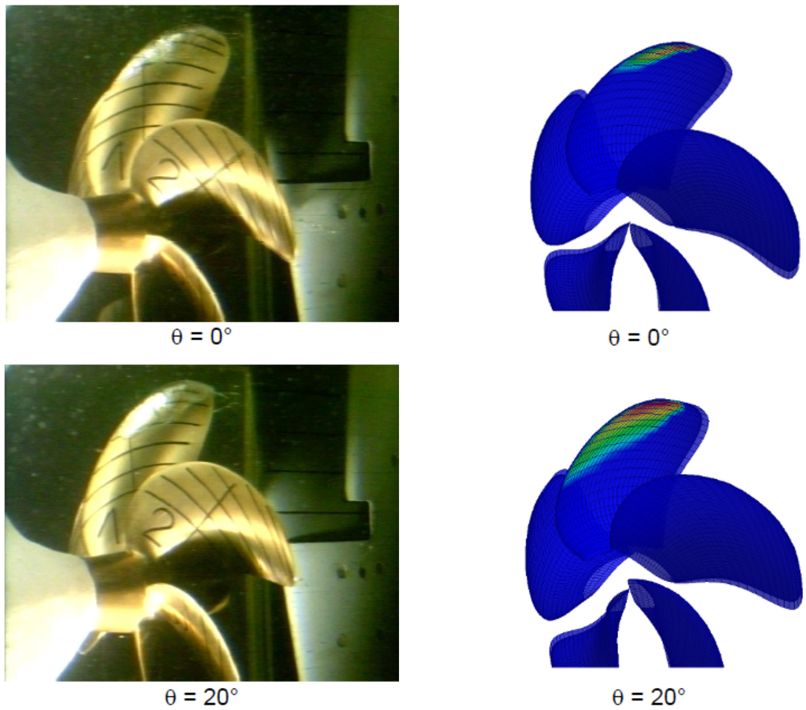

(a) Sheet cavitation measured by SVA [7]

(b) Sheet cavitation calculated by *pan*MARE

Figure 9: Comparison of the measured and calculated results for the sheet cavity shape on the KCS propeller for $\sigma_v = 2.651$ at the blade angular positions $\theta = 0°$ and $\theta = 20°$

sults [9]. Additionally, for the completeness of the sheet cavitation model, the code should be extended related to the calculation of pressure side cavitation. Pressure side cavitation occurs mainly for small angles of attack and for high cavitation numbers.

Acknowledgements

The first author is supported by the German Research Foundation (DFG) within the Research Training Group “Ports for Container Ships of Future Generations“.

References

[1] M. Bauer, M. Abdel-Maksoud, ”A 3-D Potential Based Boundary Element Method for the Modelling and Simulation of Marine Propeller Flows“, *7th Vienna Conference on Mathematical Modelling, Vienna, Austria*, 2012.

[2] J. Katz, A. Plotkin, ”Low-Speed Aerodynamics“, *Cambridge University Press, Cambridge*, 2001.

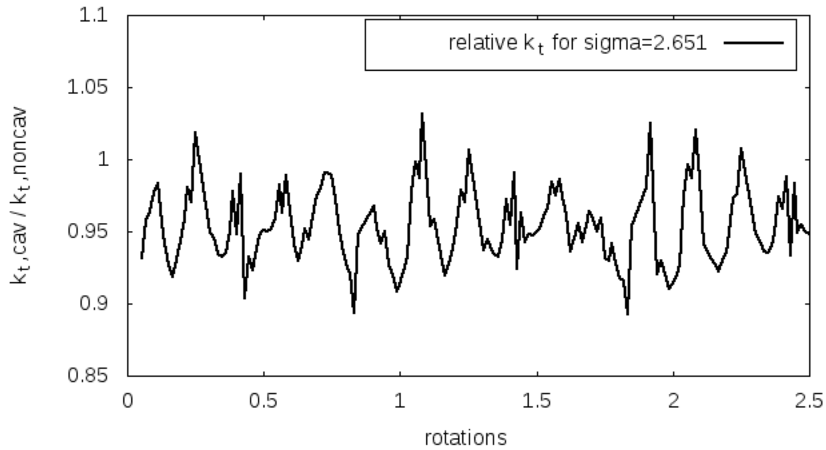

Figure 10: Relative thrust coefficient for the KCS propeller in non-uniform wakefield for $\sigma_v = 2.651$

[3] G. N. V. B. Vaz, "Modelling of Sheet Cavitation on Hydrofoils and Marine Propellers using Boundary Element Methods", *Aerospace Engineer of Instituto Superior Tecnico, Lisbon, Portugal*, 2005.

[4] S.A. Kinnas and H.S. Lee and Y.L. Young, "Modeling of unsteady sheet cavitation on marine propeller blades", *International Journal of Rotating Machinery*, 9, 263-277, 2003.

[5] H. J. de Koning Gans, "Numerical Time Dependent Sheet Cavitation Simulations using a Higher Order Panel Method", *PhD Thesis, Delft University*, Netherlands, 1994.

[6] S. Phoemsapthawee, J.-B. Leroux, J.-M. Laurens, F. Deniset. "A Transpiration Velocities Based Sheet Cavitation Model", *Ship Technology Reasearch*, 56, 191-176, 2009.

[7] H. Richter, H.-J. Heinke, "Freifahrt- und Kavitationsversuche sowie Druckschwankungsmessungen mit dem Propeller P1356 in homogener Zuströmung", *Bericht Nr. 3213*, Potsdam, 2006.

[8] H. Richter, H.-J. Heinke, "Kavitationsuntersuchungen und Druckschwankungsmessungen mit fnf Propellern am Dummymodell des KRISO Containerschiffs KS 621", *Bericht Nr. 3036*, Potsdam, 2004.

[9] S. Bal, S. A. Kinnas, "A BEM for the prediction of free surface effects on cavitating hydrofoils", *Computational Mechanics*, 28, 260-274, 2002.